ELSEVIER

Journal of Nuclear Materials 255 (1998) 92–104

journal of nuclear materials

Microstructural analysis and modelling of intergranular swelling of an irradiated UO_2 fuel treated at high temperature

I. Zacharie [a,*], S. Lansiart [a], P. Combette [b], M. Trotabas [c], M. Coster [d], M. Groos [e]

[a] *CEA / Saclay, 91191 Gif sur Yvette, France*
[b] *CEA / Siège, 75015 Paris, France*
[c] *COGEMA, 78141 Villacoublay, France*
[d] *Université de Caen, Laboratoire Lermat, 14050 Caen, France*
[e] *Ecole Centrale de Paris, Laboratoire MSS MAT, 92295 Chatenay Malabry, France*

Received 12 August 1997; accepted 18 February 1998

Abstract

Unstressed samples of uranium oxide irradiated in pressurized water reactor (PWR) fuel to a burn-up of 25 GWd/tU were subjected to thermal treatment in a laboratory furnace at temperatures of 1130°C and 1715°C for durations varying between 5 min and 10 h. They were then examined and swelling was measured. Micrographic examination of the samples showed that the bubbles were lenticular in form and intergranular. The swelling measured can be explained by bubbles coalescence alone, and a model was therefore developed. This made it possible to establish an equation for the intergranular swelling of fuel after two operating cycles as a function of time and temperature.

1. Introduction

Under normal pressurized water reactor (PWR) operating conditions, the fission products arising in the uranium oxide remain trapped in insertion or substitution in the fuel matrix. Variation of volume or swelling caused by the formation of such solid and gaseous fission products is slight and varies as a linear function of burn-up.

The situation is different if the fuel experiences a sudden power variation and is then maintained at a higher level of power for a relatively long period. Under the effect of the temperature, the fission gases precipitate and coalesce. They form bubbles of gas which cause substantial gas-induced swelling. This depends on a number of parameters: fuel characteristics, thermal gradient created, fuel burn-up, and temperature rise and hold time. In this article, the effect of hold time and temperature on irradiated PWR fuel is studied. A swelling model is then proposed to simulate the effect of these parameters in computer codes.

* Corresponding author. Tel.: +33-1 69 08 28 38; fax: +33-1 69 08 28 40; e-mail: zacharie@orgue.saclay.cea.fr.

2. Experimental aspects

2.1. The material

The samples consisted of unstressed pieces of uranium oxide a few millimetres in size, recovered when taking a section some 8 mm long.

The samples, whose main characteristics are indicated in Table 1, were derived from a UO_2 fuel rod having operated in a PWR under normal conditions for two cycles, i.e., with a burn-up of 25 GWd/tU. This fuel has the advantage of having a simple microstructure, i.e., a relatively uniform distribution of fission gases dissolved in the matrix system [1].

2.2. The thermal treatment

The treatment temperatures range from 1130°C to 1715°C and the durations vary between 5 min and 10 h, being representative of the conditions attained in the power transients created in an experimental reactor. The samples were placed in a tungsten crucible in a vacuum, then heated by induction in a high-frequency laboratory fur-

0022-3115/98/$19.00
PII: S0022-3115(98)00040-3

Table 1
Main characteristics of samples

Fuel rod	
Type of rod	UO_2
Number of cycles	2
Filling gas	He
Internal pressure (bar)	26
Fuel before irradiation	
Enrichment with U_{235} (%)	4.5
Average grain size (μm)	9.3
Density by immersion (g/cm^3)	10.39[a]
Density by immersion (% of theoretical density)	94.75
Fuel after irradiation	
Burn-up (GWd/tU)	25
Density by immersion (g/cm^3)	10.39[a]
Average grain size (μm)	9.3

[a]Densification and swelling explain that fuel before and after irradiation are the same.

nace, previously calibrated with a bichromatic optical pyrometer. The temperatures were accurate within ±20°C. The samples were loaded and unloaded at room temperature. The temperature rise time was 2.5 min and the cooling time was 2 min. Details of the treatments carried out are given in Table 2.

2.3. Metallographic preparation

Polished fractured samples, before and after thermal treatment, were observed with a scanning electron microscope. In addition to polished sample micrographs, a control sample, a sample thermally treated at 1410°C for 5 h and another at 1715°C for 5 h were fractured and analysed with a scanning electron microscope.

2.3.1. Polished samples

These were vacuum impregnated with Epoxy. They were then pre-polished in water with 200, 400 and 600 grade abrasive paper for a few minutes, then with hyprocel paper with diamond compounds of particle sizes of 8 μm and 2 μm for 20 min. Finally, flush felt was used with a 1 μm particle size solution for 1 min.

The scanning electron microscope examinations, which are shown in Fig. 1 show the presence of intergranular bubbles in virtually all the treated sample pictures. At 1410°C for 5 min and 1130°C for 300 min, hardly any boundaries can be distinguished. For the remainder of the thermal treatments, the bubbles are in sufficient quantities to localise all the grain boundaries within 5 min.

On the other hand, the intragranular bubbles, which are smaller in size, are only observable with a small number of very high temperature treatments.

To describe the development of the intergranular bubbles as a function of treatment time and temperature, the following observation criteria were adopted: the size and shape of the bubbles, the number of bubbles per unit length of grain boundary and the bubble networks.

The bubbles are lenticular in shape, and around 1 μm in size. As treatment time and temperature increases, they tend to elongate and broaden. Up to around 60 min, an increase in bubble size is observed, followed by change at a slower rate. Finally, the higher the temperature, the larger the bubbles become.

The micrographs show that as a function of time and temperature, the number of bubbles per unit length of grain boundary diminishes and the distance between the bubbles increases.

Finally, during the thermal treatments, the bubbles can combine and form channels (as can be seen in Fig. 1 eM in the area between the arrows).

2.3.2. Fractured samples

Intergranular bubbles of lenticular shape were observed, increasing in size with temperature, as well as networks of bubbles at the edges common to a number of grains (tunnels) which converge at triple-points (Fig. 2). At 1715°C, the intergranular bubbles tend to interconnect more than at 1410°C. These tunnels sometimes communicate with bubbles interconnected at the grain faces. Non-interconnected bubbles are also observed at the grain faces, increasing in size with temperature. In some cases, the tunnels pass through the initial pore (Photo C of Fig. 2).

At 1715°C, spherical intragranular bubbles are observed with an average diameter between 20 nm and 150 nm (Fig. 3). Analysis revealed an area free of intragranular bubbles in the vicinity of the grain boundaries.

Table 2
Number of bubbles per millimetre of grain boundary as a function of treatment time and temperature

$N_L(P)$	Temperature (°C)			
Time (min)	1410	1545	1630	1715
5	[a]	1700 ± 86	1320 ± 76	1052 ± 46
15				870 ± 49
30		1078 ± 99		655 ± 71
60	1015 ± 97	962 ± 92	788 ± 70	585 ± 83
120				520 ± 35
300	890 ± 56	885 ± 62	710 ± 76	492 ± 32
600		733 ± 55		464 ± 48

3. Image analysis applied to intergranular swelling determination

3.1. Processing of polished sample images

The process for determining fractions per unit volume of the porosity of untreated samples and of samples after

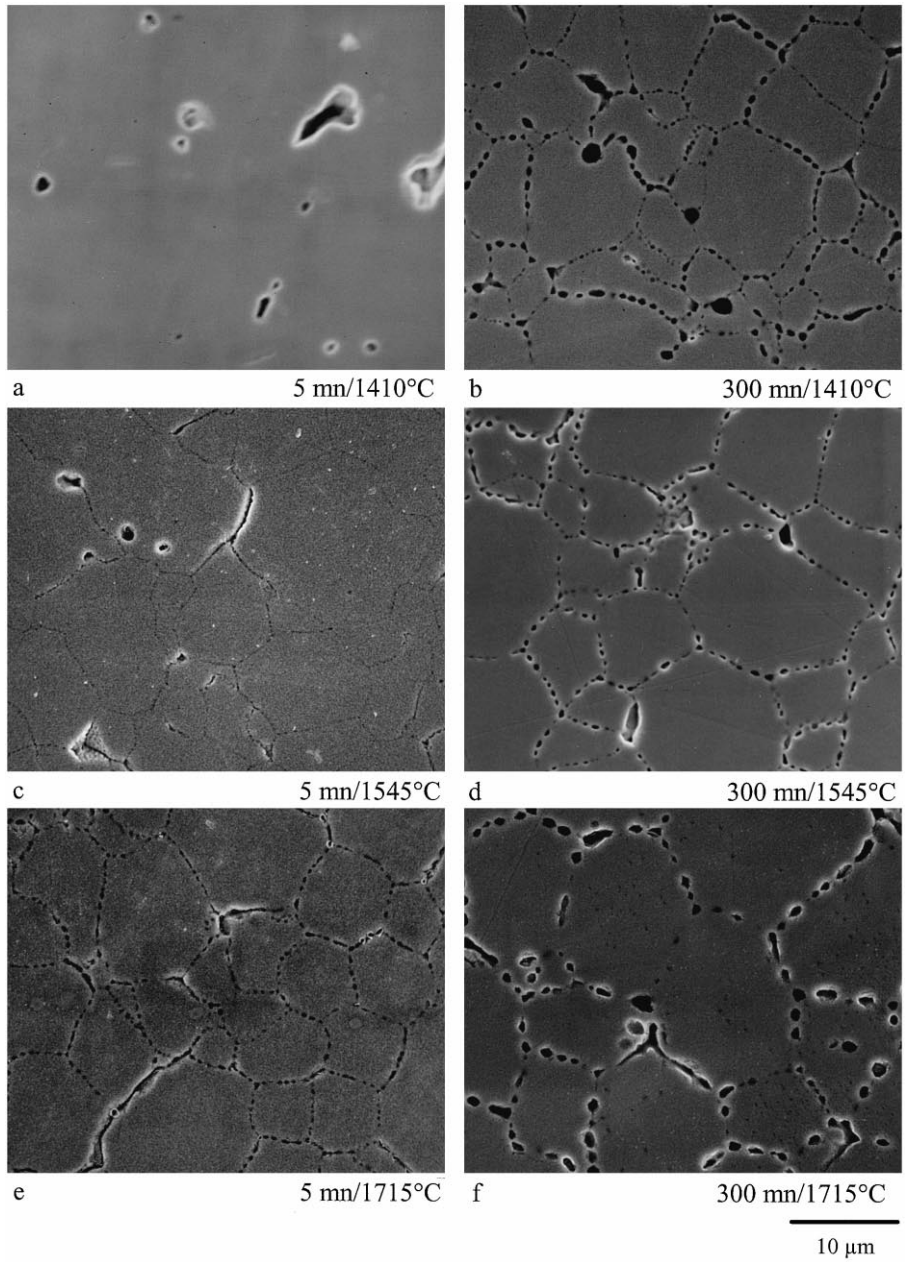

Fig. 1. Micrographic examination of samples.

thermal treatment was qualified beforehand. This consists of three stages: (A) Acquisition of grey scale images obtained from the scanning electron microscope in the back-scatter mode with polished sections (Fig. 4). The section analysed is restricted to a window representative of the entire surface corresponding to 150 images, at magnification of 2000 and 3500. (B) Thresholding the images to make measurements and counts. To obtain the binary image, a method of automatic thresholding based on analysis of the grey scale histogram data is used. Of the different available methods, that one which maximises the entropy of the image [1] gives the best results. (C) Processing of the binary images: to eliminate the background noise of the binary image, the images are filtered by an open/reconstruct operation. Furthermore, to minimise the effect of defects (grain pick-up), an open/reconstruct op-

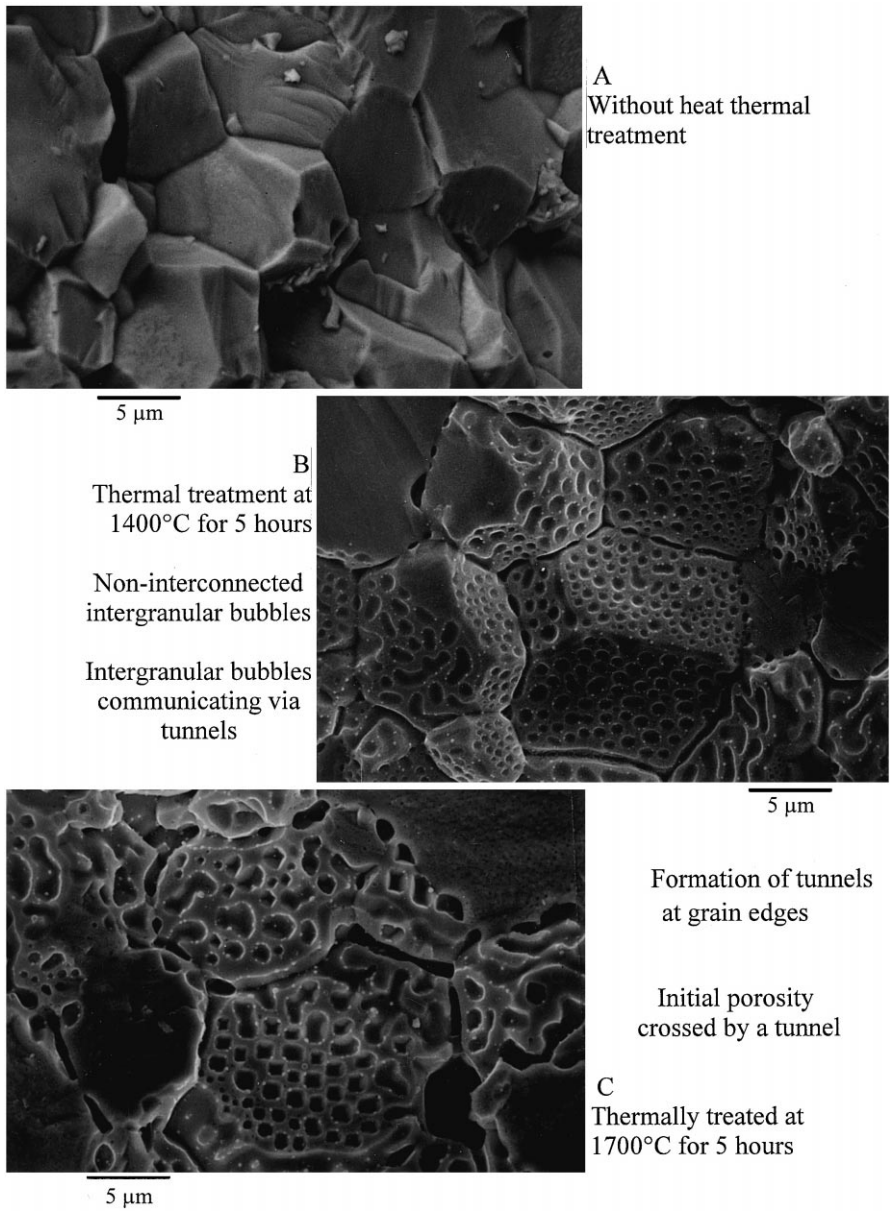

Fig. 2. Scanning electron microscope examination of fracture samples (25 GWd/tU) with and without thermal treatment: Intergranular bubbles–bubble interconnection–tunnels.

eration is performed for a size of 3.2 μm to eliminate large elements which do not participate in swelling [2].

3.2. Analysis

3.2.1. Measurement of porosity

Automatic analysis essentially related to variation of the degree of porosity $A_A(P)$. According to the stereological relationship $A_A(P) = V_V(P)$ [1], it was possible to determine the swelling of the material using the following formula:

$$S_3 = \frac{V_v(P)_{(f)} - V_v(P)_{(i)}}{1 - V_v(P)_{(f)}} = \frac{A_A(P)_{(f)} - A_A(P)_{(i)}}{1 - A_A(P)_{(f)}}, \quad (1)$$

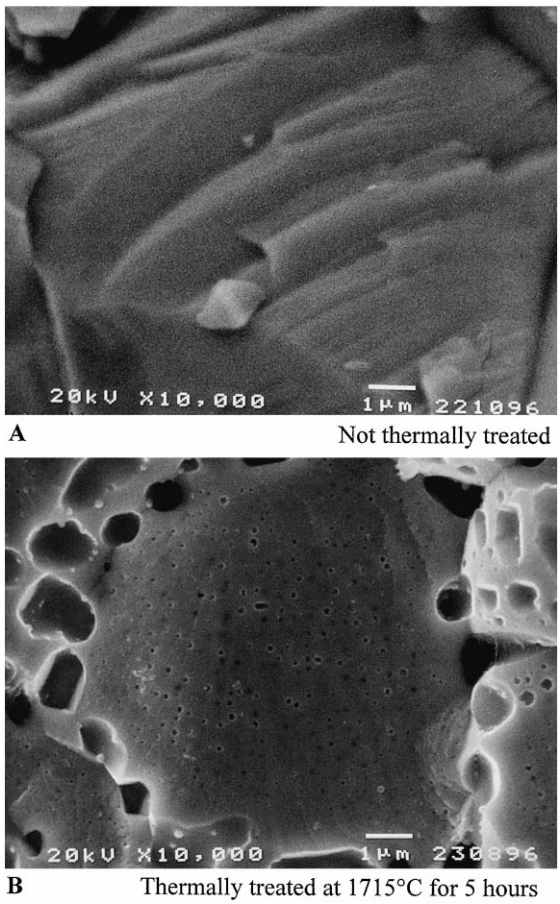

Fig. 3. Formation of intergranular bubbles in a fractured sample (25 GWd/tU) treated at 1715°C for 5 h.

where $V_V(P)_{(i)}$ and $V_V(P)_{(f)}$ are the volume-related porosity factors before and after treatment, respectively, $A_A(P)_{(i)}$ and $A_A(P)_{(f)}$ are the area-related porosity factors

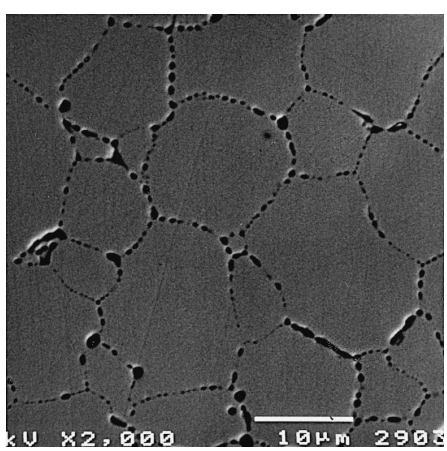

Fig. 4. Back-scatter mode image of a two-cycle UO_2 specimen treated at 1545°C for 1 h.

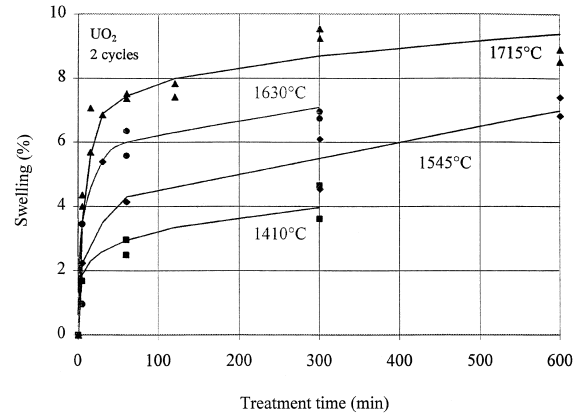

Fig. 5. Intergranular swelling as determined by image analysis, as a function of treatment time at different temperatures.

before and after treatment, respectively. Accuracy of measurement is estimated at $\pm 1\%$.

It is to be noticed that the swelling determined by electronic image analysis only covers bubbles of thicknesses greater than 0.1 µm. As bubbles of smaller sizes are essentially intragranular, image analysis provides a measurement of swelling of intergranular origin. The results are shown in Fig. 5.

3.2.2. Measurement of grain size

Grain size was not measured by an automatic grain segmentation method. We used standard ASTM E112-88 which enabled us to evaluate the average size and to demonstrate that this average grain size (measured with an optical microscope) does not change with the thermal treatments. This was equal to 9.3 ± 0.3 µm.

3.2.3. Number of bubbles per unit grain boundary length

As we did not segment the grain boundary network using an automatic method, the measurements of the num-

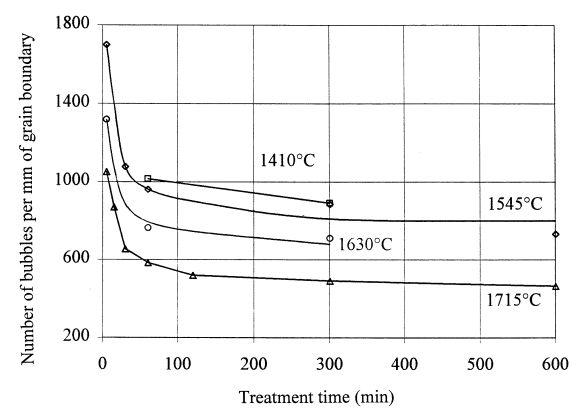

Fig. 6. Number of bubbles per millimetre of grain boundary, as a function of treatment time, at different temperatures.

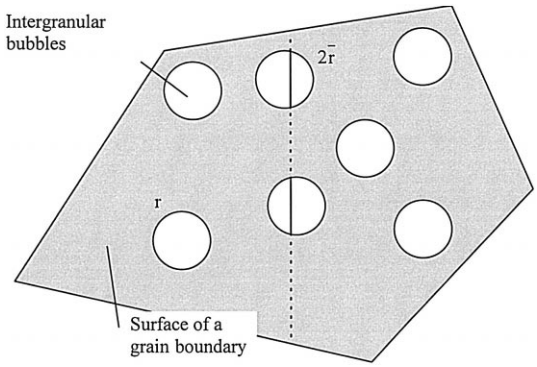

Fig. 7. Surface of a grain boundary.

ber of bubbles per unit grain boundary length were made manually from photographs. The number of bubbles per unit grain boundary length measured is designated $N_L(P)$. The results are shown in Table 2.

The curves as a function of time in Fig. 6 show in quantitative form the observations made in Section 2.3.1. These are of identical shape, for each temperature. During an initial phase lasting 60 min, the number of bubbles per unit grain boundary length diminishes considerably; this phenomenon then slows down. Furthermore, for a given treatment time, the number of bubbles per unit grain boundary length decreases with temperature.

3.2.4. Bubbles size

Determination of the size of an object in $\Re^3$ is a stereological problem with no general solution without hypothesising or modelling. In our case, we considered an average uniform bubble size. With this hypothesis, from the measurements of the number of bubbles per unit grain boundary length $N_L(P)$ and the measurements of swelling G by image analysis, the variation of radius r of the average area of boundary occupied by lenticular bubbles (r is defined in Fig. 7) was deduced. Calculation will be discussed next.

· First, the relationship was sought between the bubble concentration $N_v(P)$ and the number of bubbles per unit grain boundary length $N_L(P)$. Using the calculations given in Appendix A, the following was obtained:

$$N_v(P) = \frac{2}{\bar{\ell}} \frac{N_L(P)}{\rho \sin\Psi}, \tag{2}$$

where ρ is the average radius of curvature (Fig. 8) and Ψ the contact angle. The average grain size $\bar{\ell}$ remains virtually constant with irradiation and thermal treatments. It is taken to be equal to the initial size of the grain, before irradiation and before thermal treatment, i.e., 9.3 μm. Furthermore, angle Ψ of encounter of the two halves of the cavity is approximately equal to 56° [6].

· Furthermore, intergranular swelling is equal to the product of the concentration per unit volume of intergranular bubbles and the average volume of a lenticular bubble:

$$G = N_v(P)\,\bar{V}. \tag{3}$$

The volume of a lenticular bubble is given by the equation

$$\bar{V} = F_v \rho^3, \tag{4}$$

where [5]

$$F_v = \frac{2\pi}{3}(1-\cos\Psi)^2(2+\cos\Psi).$$

By substituting relationship (2) for $N_v(P)$ and for Eq. (4) volume V in Eq. (3), bubble radius of curvature is obtained:

$$\rho = \left(\frac{\bar{\ell} \sin\Psi\, G}{2 F_v N_L(P)} \right)^{1/2}.$$

However, the average radius r of the boundary area taken up by the cavity (Fig. 5) is given by

$$r = \rho \sin\Psi;$$

hence

$$r = \left(\frac{\bar{\ell} \sin\Psi\, G}{2 F_v N_L(P)} \right)^{1/2} \sin\Psi. \tag{5}$$

· Bubble size variation was thus deduced and the corresponding curves are shown in Fig. 9. It can be seen

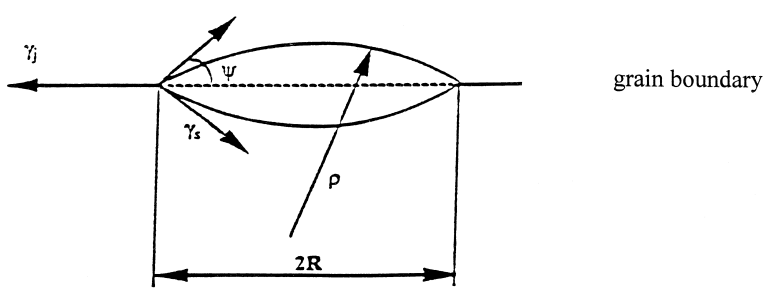

Fig. 8. Diagram of a lenticular bubble at a grain boundary with an energy of γ_j when the surface energy is γ_s.

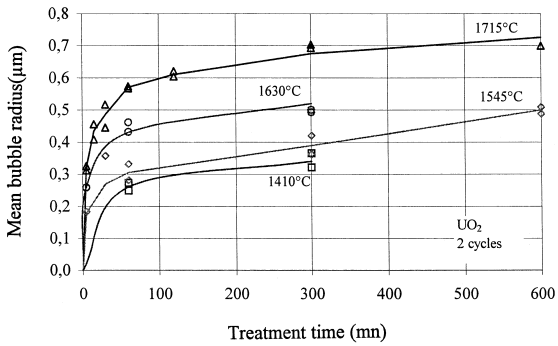

Fig. 9. Mean radius of grain boundary bubble as a function of treatment time, at different temperatures.

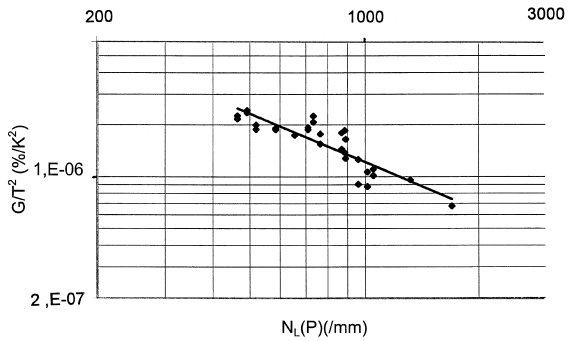

Fig. 10. Intergranular swelling of treated samples, against squared temperature, as a function of the number of bubbles per 1 mm of grain boundary.

that bubble size increases substantially for around 60 min, followed by a second phase when it varies more slowly. The higher the temperature, the greater the size.

The values which we obtained at 1715°C and 5 h are comparable with those that Kashibe and Une [7] measured in irradiated UO_2 fuel (25 GWd/tU) thermally treated at 1800°C for 5 h. Bubble sizes vary between 0.6 and 0.8 μm.

4. Interpretation of intergranular swelling

To analyse intergranular swelling, we considered to determine the phenomenon or phenomena which control intergranular swelling, at high temperatures. We then established a theoretical model for which an equation was derived linking swelling to treatment time and temperature. Finally, the equation was validated with experimental results.

4.1. Growth by coalescence and / or absorption of atoms

The micrographs, as well as the measurements made, indicated a decrease in the number of bubbles per unit grain boundary length and an increase in bubble size with treatment time and temperature. Furthermore, the distance between the bubbles increased. The observations suggested a coalescence phenomenon.

It is to be noted that no increase in the number of small bubbles with treatment time was observed, which could have indicated continuous germination.

The question then arose as to whether this mechanism of coalescence predominates in intergranular swelling or whether it is in competition with bubble growth by in-grain atom absorption.

Assuming that coalescence is the main mechanism controlling intergranular bubble growth, we determined the theoretical relationship between intergranular swelling G and the number of bubbles per unit grain boundary length $N_L(P)$ and examined whether the experimental data agreed with these laws. During coalescence of intergranular bubbles, the number of gas atoms M, trapped in the grain boundary area remains constant. For the purpose, a perfect gas was considered associated with lenticular bubbles in equilibrium. The calculations shown in Appendix B gave

$$\frac{G}{T^2} = \frac{A}{N_L(P)} \tag{6}$$

which is equivalent to

$$\log(G/T^2) = \log A - \log(N_L), \tag{7}$$

where

$$A = \left(\frac{Mk}{\gamma_s}\right)^2 \frac{2}{\bar{\ell} F_v} \sin\Psi = \text{constant},$$

where M is the number of fission gas atoms per unit grain boundary area, γ_s the surface tension and F_v the shape factor for the volume of the bubble.

Fig. 10 shows the experimental relationship between intergranular swelling against temperature and the number of bubbles per unit grain boundary length against temperature. The experimental data describe a straight line, for which the corresponding equation obtained by linear regression from the data points is as follows:

$$\log\frac{G(\%)}{T} = -0.9\log Nj(/\text{mm})/T + 0.1.$$

The slope of -0.9 is virtually equal to the factor of -1 proposed in the theoretical relationship (6). The coefficient A is equal to 1.3 (%mm). The theoretical relationship and the experimental readings thus agree. The hypothesis of bubbles coalescence in intergranular swelling thus appeared to be borne out.

4.2. Model for swelling by coalescence of bubbles

We considered it is necessary to establish a theoretical model, based on the phenomenon of coalescence.

The initial hypotheses were those proposed by Greenwood and Speight [8]. The fission gas atoms in the matrix were created by prior irradiation in a nuclear reactor at a relatively low temperature. At the initial instant of heat treatment, the fission gas atoms precipitated instantaneously at the grain boundaries to form N_0 seeds per unit grain boundary area, of radius ρ_0.

The gas was considered to be perfect.

It was assumed that intergranular swelling was due to the phenomenon of bubbles coalescence alone (and therefore the growth of bubbles by absorption of atoms originating from inside the grains was disregarded). During heat treatment, bubbles become mobile and it was considered that they migrated at random, i.e., that there was no mutual attraction between them. When two bubbles meet, they merge and to re-establish its equilibrium the new bubble immediately absorbs openings, the number of which depends on the size of the bubble. Over time, the number of bubbles diminishes and the size of the bubbles increases.

Bubbles located at grain boundaries are not spherical but lenticular, with a radius of curvature ρ.

We planned to establish the equation for intergranular swelling as a function of the treatment time and temperature, calculated on the basis of the radius of curvature.

Unlike in the Greenwood and Speight model, we did not determine the rate of bubbles coalescence, nor did we make any hypotheses concerning the mechanism causing random migration of the bubbles.

The variation of the radius of curvature was examined by dividing the time into different intervals Δt such that, during each Δt time increment, each bubble migrates and at the end of the Δt event, each bubble coalesces with another neighbouring one. Thus there was no coalescence of bubbles during interval Δt, but only at the end of the interval.

The start of the interval Δt was designated t_i and the end of the interval was designated t_{i+1}. Between t_i and t_{i+1}, the radius was equal to r_i and at time t_{i+1}, changes on coalescence from ρ_i to ρ_{i+1} (Fig. 11).

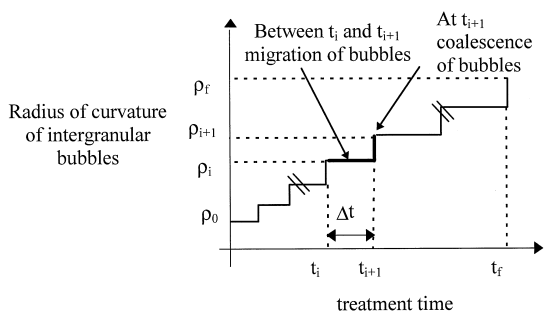

Fig. 11. Diagram of the variation of the radius of curvature of intergranular bubbles as a function of time, during thermal treatment.

1. Bubble movement is Brownian. During a time $\Delta t = t_{i+1} - t_i$, a bubble moves over the grain surface by a distance $\bar{x}$, equivalent to the mean quadratic path of the bubble and defined by [9]

$$\bar{x} = (4D_b \Delta t)^{1/2} = \left(4D_b(t_{i+1} - t_i)\right)^{1/2},$$

where D_b is the bubble diffusion coefficient, considered in points as bubble size dependent.

This can also be expressed as follows:

$$t_{i+1} - t_i = \frac{\bar{x}^2}{4D_b}. \tag{8}$$

2. During the time $\Delta t = t_{i+1} - t_i$, the bubble moves a distance $\bar{x}$ without encountering other bubbles. Each section $\pi \bar{x}^2$ of the grain boundary surface only contains a single bubble. The number of bubbles per unit grain boundary surface area $N_s(P)$ is thus

$$N_s(P) = \frac{1}{\pi \bar{x}^2};$$

hence

$$\bar{x}^2 = \frac{1}{\pi N_s(P)}. \tag{9}$$

3. At time t_{i+1}, each bubble encounters its neighbour and coalesces with it. The radius changes from ρ_i to ρ_{i+1}. On coalescence of the bubbles, the sum of the areas of the bubbles is conserved and the area of a bubble of radius of curvature ρ is equal to $F_s \rho^2$ where F_s is equal to $4\pi(1 - \cos\psi)$ and ψ is the angle of encounter of the two halves of the cavity [5]. Merging of two identical bubbles of area S_1 results in one bubble of area S_2 defined by

$$S_2 = 2S_1$$

which is equivalent to

$$F_s(\rho_{i+1})^2 = 2F_s \rho_i^2;$$

hence

$$\rho_{i+1} = \sqrt{2}\,\rho_i. \tag{10}$$

The progression ρ is therefore geometrical and $\sqrt{2}$ based. It can also be written as

$$\rho_i = \sqrt{2}^{(i-f)} \rho_f, \tag{11}$$

where ρ_f is the radius of curvature of the bubble at t_f.

The variation of the radius of curvature $\Delta\rho$ is then

$$\Delta\rho = \rho_{i+1} - \rho_i = \left(\sqrt{2} - 1\right)\rho_i. \tag{12}$$

4. On coalescence of the bubbles, the number of bubbles per unit grain boundary area and the radius of curvature ρ_i are linked by the relationship (Eq. (2)).

5. It is considered that the larger the bubble, the slower it moves. It is therefore proposed to introduce into the diffusion coefficient the term ρ_i^q where $q > 1$. The effect of temperature is represented by the law of Arrhenius.

Bubble diffusion coefficient D_b is therefore assumed to be of the following form:

$$D_b = D_0 \exp\left(\frac{-Q}{RT}\right)\frac{1}{\rho_i^q}, \qquad \text{where } q > 1. \tag{13}$$

The radius of curvature calculation is given in Appendix C. This gives the relationship

$$\rho = \left(\frac{4\pi\left(\sqrt{2}^{q+2}-1\right)D_0 M}{F_v}\,\frac{k}{2\gamma_s}T\exp\left(\frac{-Q}{RT}\right)t\right)^{1/q+2}. \tag{14}$$

Radius of curvature and swelling are thus linked as follows:

$$\frac{G}{T} = \frac{2}{\bar{\ell}}\frac{Mk}{\gamma_s}\rho.$$

Swelling in terms of temperature becomes

$$\frac{G}{T} = \frac{Mk}{2\gamma_s}\frac{2}{\bar{\ell}}\left(\frac{4\pi\left(\sqrt{2}^{q+2}-1\right)D_0 M}{F_v} \times \frac{k}{2\gamma_s}T\exp\left(\frac{-Q}{RT}\right)t\right)^{1/q+2}.$$

It is of the following form:

$$\frac{G}{T} = D\left(t\,T\exp\left(\frac{-Q}{RT}\right)\right)^{1/q+2}, \tag{15}$$

where

$$D = \frac{Mk}{\gamma_s}\frac{2}{\bar{\ell}}\left(\frac{4\pi\left(\sqrt{2}^{q+2}-1\right)D_0 M}{F_v}\,\frac{k}{2\gamma_s}\right)^{1/q+2}, \tag{16}$$

G is swelling, T is temperature, t is treatment time, Q is apparent activation energy, R is perfect gas constant, M is number of fission gas atoms per unit, k is Boltzmann's constant, grain boundary area, γ_s is surface tension, $\bar{\ell}$ is grain size, D_0 is Arrhenius law frequency factor, F_v is factor proportional to volume of bubble.

It is to be noted that this equation is only valid when $f \geq 1$, i.e., when a Δt interval has elapsed.

A theoretical model is thus obtained, based on bubbles coalescence, with processing time and temperature as parameters.

4.3. Comparison of the theoretical model with the experimental data points

Let us now see how the experimental values for intergranular swelling compare to the above theoretical model and assess coefficient q (expressing the speed of the bubbles) as well as apparent activation energy Q of the intergranular swelling mechanism. This will make possible to obtain a semi-empirical law for intergranular swelling.

4.3.1. Effect of treatment time

According to the model previously developed, variation of intergranular swelling as a function of temperature is given by the formula (15).

Let

$$C_T = DT^{1/q+2}\exp\left(\frac{-Q}{RT(q+2)}\right).$$

Swelling with temperature can thus be written as

$$\frac{G}{T} = C_T\, t^{1/q+2}.$$

Fig. 12 shows intergranular swelling with temperature as a function of treatment time (logarithmic coordinates).

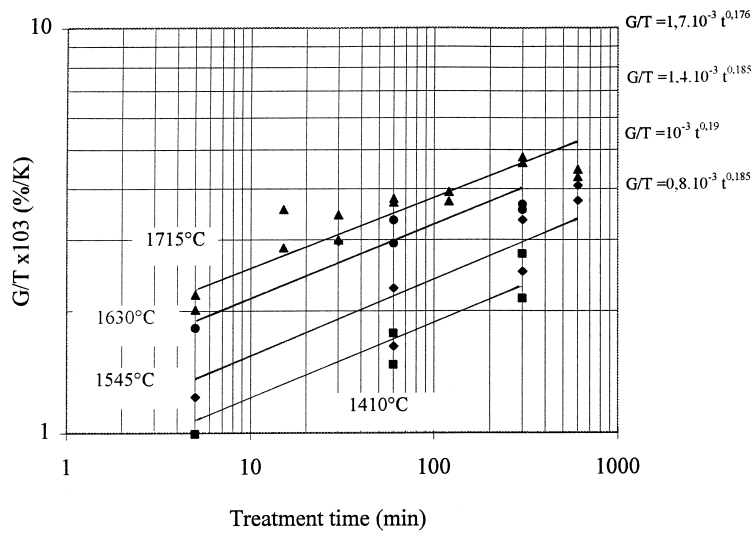

Fig. 12. Intergranular swelling of treated samples against temperature as a function of treatment time, for different temperatures (logarithmic coordinates).

Table 3
Coefficient C_T as a function of temperature

Temperature (°C)	C_T (%/K $s^{1/5.4}$)
1410	0.381×10^{-3}
1545	0.52×10^{-3}
1630	0.625×10^{-3}
1715	0.743×10^{-3}

If a linear regression is made, for each temperature and for all the experimental data points, parallel straight lines are obtained. This would appear to validate the form proposed as a function of time, for all the treatments. It is then possible to determine coefficient $1/q+2$ which is equal to the average of the slopes of different curves. The following is found:

$1/q+2=0.185$, hence $q=3.4$.

An analogy can be drawn with the theoretical intragranular mechanisms for random migration which indicate powers of 3 and 4 [10].

By replacing $q+2$ by its value, swelling can be written as follows:

$$\frac{G}{T}=C_T\,t^{1/5.4}.$$

Coefficient C_T is determined for different temperatures by plotting swelling against temperature as a function of time and power $(1/5.4)$, then by making a linear regression of the experimental data points through the origin. The coefficients C_T thus obtained are given in Table 3.

4.3.2. Effect of temperature

Let us now study the effect of the temperature covered with coefficient C_T. This can be written as follows:

$$C_T=DT^{1/q+2}\exp\left(\frac{-Q}{RT(q+2)}\right);$$

hence

$$\frac{C_T}{T^{1/q+2}}=D\exp\left(\frac{-Q}{RT(q+2)}\right).$$

Fig. 13 gives $C_T/T^{1/5.4}$ as a function of $1/T$. The experimental data points are aligned and thus bear out the relationship suggested. Throughout the temperature range, bubbles coalescence is therefore the only predominant mechanism in swelling. The slope of the straight line is equal to $[-QR(5.4)]$, which makes it possible to determine Q:

$Q=310\,\mathrm{kJ/mol}$.

This activation energy of 310 kJ, which corresponds to a migration of intergranular bubbles, is, as expected, lower than the 540 kJ (5.6 eV) activation energy of migration of bubbles in the grain [11]. This energy is, furthermore, higher than the 239 kJ activation energy for self-diffusion

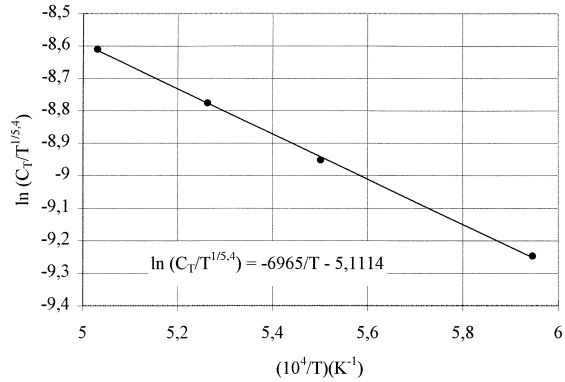

Fig. 13. Variation of the Napierian logarithm of coefficient $C_T/T^{1/5.4}$ as an inverse function of temperature.

of the uranium at the grain boundaries, proposed by Reynolds and Burton [12].

The swelling equation can therefore be written as follows:

$$\frac{G}{T}=Dt^{1/5.4}T^{1/5.4}\exp\left(\frac{-310\times10^3}{RT}\right)^{1/5.4}$$

or otherwise as a function of a parameter $H=tT\exp((-310\times10^3)/(RT))$

$$\frac{G}{T}=DH^{1/5.4}.$$

G/T as a function of H is shown in Fig. 14. The experimental data points are grouped around the theoretical curve. It is thus possible to determine the factor D:

$D=0.0061\left(\%/\mathrm{K}^{6.4/5.4}\,\mathrm{s}^{1/5.4}\right)$.

Finally, the free swelling equation becomes

$$\frac{G}{T}=0.0061t^{1/5.4}T^{1/5.4}\exp\left(\frac{-310\times10^3}{RT}\right)^{1/5.4}.$$

This reasoning thus makes it possible to suggest the semi-empirical law for intergranular swelling. Swelling G

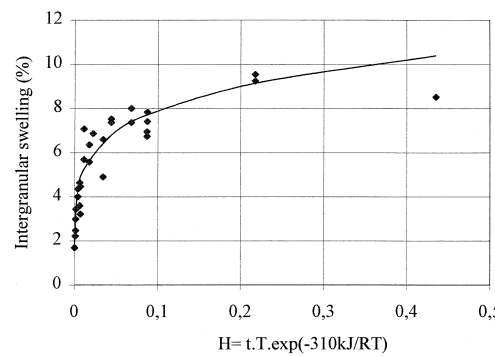

Fig. 14. Intergranular swelling of treated samples against temperature as a function of treatment time corrected for the effect of temperature.

is expressed in %, temperature in K, and processing time in s. The perfect gas constant R is equal to 8.314 J/mol K.

The equation can be used for treatment times between 5 min and 10 h and temperatures of 1410°C and 1715°C. It only applies to UO_2 fuel with 25 GWd/tU irradiation in a PWR.

5. Conclusion

Different unstressed samples of UO_2 taken from PWR fuel after two cycles under normal conditions, i.e., with a burn-up of 25 GWd/tU, were treated in a laboratory furnace at temperatures between 1100°C and 1700°C for periods of between 5 min and 10 h. The intergranular swelling was measured. The main findings are explained in this section.

Intergranular swelling as a function of treatment time and temperature was monitored. At all the temperatures, there was found to be a rapid increase for the first 60 min of treatment, followed by slow growth thereafter. The effect of temperature is significant and swelling increases with temperature.

This process was also observed on quantitative and qualitative analysis of the microstructure of the samples with a scanning electron microscope, as a function of time and of temperature. There was found to be a rapid increase, in the first 60 min, in the average size of the bubbles as well as a reduction in the number of bubbles per unit grain boundary length, followed by a slower change.

Micrographic examination of the samples, after thermal treatments, showed that the bubbles were intergranular and lenticular in shape. As time and temperature increased, the size of the bubbles increases and their number, per unit boundary length, decreases while the space between them increases. At this stage, the phenomenon of bubbles growth by absorption of fission gas atoms originating from inside the grains and the phenomenon of bubbles coalescence were considered to explain these observations. A calculation showed that the swelling measured can be explained by bubble coalescence alone, without it being necessary to consider their growth by absorption of fission gas atoms (gas atoms which arrive by diffusion in the grain boundary, are probably evacuated to the exterior and do not participate in swelling).

On the basis of the phenomenon of coalescence revealed in micrographic examination, a numerical model was developed. This model led to an equation giving intergranular swelling as a function of temperature and time. This was adjusted to experimental readings of swelling. These made it possible to establish the constants of the following equation:

$$\frac{G}{T} = 0.0061 t^{1/5.4} T^{1/5.4} \exp\left(\frac{-310\times 10^3}{RT}\right)^{1/5.4},$$

where G is swelling (%), T is temperature (K), t is treatment time (s), R is perfect gas constant ($R = 8.314$ J/mol K).

This equation represents the phenomenon of free intergranular swelling of fuel irradiated by 25 GWd/tU in a PWR. It is valid for treatment times between 5 min and 10 h and temperatures of 1100°C to 1700°C.

Appendix A

Given that grain boundaries are distributed at random in the material, it can be stated that the fraction per unit area of the bubbles trapped in the grain boundaries is equal to the linear fraction of the bubbles trapped in the grain boundaries [1–4]. This can be written as follows:

$$N_s(P)\pi r^2 = N_L(P) 2\bar{r}, \tag{A.1}$$

where $\bar{r}$ is the mean half cord of the cross-section of the bubble, r the radius of the cross-section of the bubbles at the grain boundary, $N_s(P)$ the number of bubbles per unit of grain boundary area and $N_L(P)$ the number of bubbles per unit of grain boundary length. Furthermore, the mean cord is defined by

$$\bar{r} = \frac{\pi}{4} r.$$

By replacing $\bar{r}$ in Eq. (1), the following is obtained:

$$N_s(P) = \frac{N_L(P)}{2r}.$$

However, for a lenticular bubble, as schematically shown in Fig. 8, r and ρ the radius of curvature of the bubble are linked as follows:

$$r = \rho \sin\Psi,$$

where

$$N_s(P) = \frac{N_L(P)}{2\rho\sin\Psi}. \tag{A.2}$$

Bubble concentration $N_v(P)$ and the number of bubbles per unit grain boundary area $N_s(P)$ are linked by the relationship

$$N_v(P) = S_v(J) \times N_s(P),$$

where $S_v(P)$ is the specific area of the grain boundaries. Under the hypotheses, $S_v(J)$ can be written [1]:

$$S_v(J) = 4\, N_L(J)$$

where $N_L(J)$ is equal to the reciprocal of the grain size $\bar{\ell}$. Hence

$$N_v(P) = \frac{4}{\bar{\ell}} N_s(P).$$

By replacing $N_s(P)$ by the formula (III.7), the following is obtained:

$$N_v(P) = \frac{2}{\ell} \frac{N_L(P)}{\rho \sin\Psi}.$$

Appendix B

Let us therefore assume that swelling is due to coalescence alone. When intergranular bubbles combine, the number of atoms of fission gas trapped at the grain boundary surface remains constant. The conservation of the number of fission gas atoms can be written:

$$nN_s(P) = M = \text{constant}, \tag{B.1}$$

where n is the number of fission gas atoms per bubble, $N_s(P)$ the number of bubbles per unit grain boundary area and M the total number of fission gas atoms per unit grain boundary area.

The number of atoms, n, of fission gas per bubble is given by the perfect gas equation. Considering the bubbles in equilibrium, the Eq. (B.1) can be written as follows:

$$N_s(P)\rho^2 = \left(\frac{MkT}{F_v 2\gamma_s}\right). \tag{B.2}$$

However, the number of bubbles per unit area $N_s(P)$ is linked by Eq. (A.2) to the number of bubbles $N_L(P)$ per unit grain boundary length. Eq. (B.2) becomes

$$\rho = \left(\frac{MkT \sin\psi}{F_v \gamma_s}\right) \frac{1}{N_L(P)}. \tag{B.3}$$

Intergranular swelling is, furthermore, equal to the product of the average volume of a bubble and the concentration per unit volume in the bubbles $N_v(P)$:

$$G = VN_v(P).$$

According to Eqs. (2) and (4) for the volume of a lenticular bubble, this becomes

$$G = F_v \rho^2 \frac{2}{\ell} \frac{N_L(P)}{\sin\psi}. \tag{B.4}$$

By introducing Eq. (B.3) into Eq. (B.4), intergranular swelling and the number of bubbles per unit grain boundary length are linked by

$$G = \left(\frac{MkT}{\gamma_s}\right)^2 \frac{2}{\ell F_v} \frac{\sin\psi}{N_L(P)}. \tag{B.5}$$

Appendix C

According to Eqs. (8) and (10), the relationship $(\rho_i + 1 - \rho_i)/(t_{i+1} - t_i)$ can be written as follows:

$$\frac{\rho_{i+1} - \rho_i}{t_{i+1} - t_i} = \frac{4D_b(\sqrt{2} - 1)\rho_i}{\bar{x}^2}.$$

If D_b is replaced by Eq. (13) and $\bar{x}$ by Eq. (9), the following is obtained:

$$\frac{\rho_{i+1} - \rho_i}{t_{i+1} - t_i} = \frac{4D_0 \exp\left(\frac{-Q}{RT}\right) \frac{1}{\rho_i^q} (\sqrt{2} - 1)\rho_i}{1/\pi N_s}.$$

However, $N_s(P)$ is given by Eq. (B.2), therefore

$$\frac{\rho_{i+1} - \rho_i}{t_{i+1} - t_i} = \frac{4\pi(\sqrt{2} - 1) D_0 M}{F_v} \frac{k}{2\gamma_s} T \exp\left(\frac{-Q}{RT}\right) \frac{1}{\rho_i^{q+1}}.$$

This equation is of the following form:

$$\frac{\rho_{i+1} - \rho_i}{t_{i+1} - t_i} = K(T) \frac{1}{\rho_i^{q+1}}, \tag{C.1}$$

where

$$K(T) = \frac{4\pi(\sqrt{2} - 1) D_0 M}{F_v} \frac{k}{2\gamma_s} T \exp\left(\frac{-Q}{RT}\right). \tag{C.2}$$

By replacing ρ_{i+1} by Eq. (10) and ρ_i by Eq. (11) Eq. (C.1) becomes

$$(\sqrt{2} - 1)\sqrt{2}^{-(i-f)(q+2)} \rho_f^{(q+2)} = K(T)(t_{i+1} - t_i). \tag{C.3}$$

We now sum all the Δt time intervals which elapse so as to determine the variation of the radius of curvature ρ_f at t_f. At each instant t_f, f increments Δt have elapsed, during which the radius has varied from ρ_o to ρ_f. The time origin is t_0:

$$\sum_{i=0}^{f-1} (t_{i+1} - t_i) = t_f \qquad \text{where } f \geq 1.$$

By summing Eq. (C.3) from 0 to $f-1$, the following is obtained:

$$\left(\sqrt{2}-1\right)\rho_f^{(q+2)}\sqrt{2}^{(-f)(q+2)}\sum_{i=0}^{f-1}\sqrt{2}^{(i)(q+2)}=K(T)t_f. \tag{C.4}$$

However

$$\sum_{i=0}^{f-1}\sqrt{2}^{(i)(q+2)}=\frac{1-\sqrt{2}^{f(q+2)}}{1-\sqrt{2}^{q+2}}. \tag{C.4a}$$

By inserting Eq. (C.4) into Eq. (C.3), the following is obtained:

$$\left(\sqrt{2}-1\right)\rho_f^{(q+2)}\sqrt{2}^{(-f)(q+2)}\frac{1-\sqrt{2}^{f(q+2)}}{1-\sqrt{2}^{q+2}}=K(T)\,t_f.$$

For $t\geq 2{,}3$, the term $1/\sqrt{2^{f(q+2)}}$ is negligible with respect 1.

$$\rho_f^{(q+2)}=\frac{\left(\sqrt{2}^{q+2}-1\right)}{\left(\sqrt{2}-1\right)}K(T)t_f.$$

By replacing $K(T)$ by the expression Eq. (C.2)

$$\rho_f^{(q+2)}=\frac{4\pi\left(\sqrt{2}^{q+2}-1\right)D_0M}{F_v}\frac{k}{2\gamma_s}T\exp\left(\frac{-Q}{RT}\right)t_f$$

which is equal to

$$\rho_f=\left(\frac{4\pi\left(\sqrt{2}^{q+2}-1\right)D_0M}{F_v}\frac{k}{2\gamma_s}T\exp\left(\frac{-Q}{RT}\right)t_f\right)^{1/q+2}.$$

The radius ρ_f at time t_f corresponds to radius ρ at time t:

$$\rho=\left(\frac{4\pi\left(\sqrt{2}^{q+2}-1\right)D_0M}{F_v}\frac{k}{2\gamma_s}T\exp\left(\frac{-Q}{RT}\right)t\right)^{1/q+2}.$$

References

[1] M. Coster, J.L. Chermant, Précis d'analyse d'images, Presses du CNRS, 1989.
[2] I. Zacharie, PhD thesis, Traitements thermiques de l'oxyde d'uranium irradié en réacteur à eau pressurisée, Gonflement et relâchement des gaz de fission, Ecole Centrale Paris, 1997.
[3] J. Serra, Image Analysis and Mathematical Morphology, Academic Press, London, 1982.
[4] R.T. Dehoff, F.N. Rhines, Microscopie Quantitative, Masson, 1972.
[5] D. François, A. Pineau, A. Zaoui, Comportement mécanique des matériaux, viscoplasticité, endommagement, mécanique de la rupture, mécanique de contact, Hermès, Paris, 1993.
[6] K. Une, J. Nucl. Mater. 158 (1988) 188.
[7] S. Kashibe, K. Une, J. Nucl. Sci. Technol. 28 (12) (1991) 1090.
[8] G.W. Greenwood, M.V. Speight, J. Nucl. Mater. 10 (2) (1963) 140.
[9] J.A. Turnbull, J. Nucl. Mater. 62 (1976) 325.
[10] D. Olander, Fundamental Aspects of Nuclear Reactor Fuel Elements, ERDA Technical Information Center, Oak Ridge, TN, USA, 1976.
[11] M.E. Gulden, J. Nucl. Mater. 23 (1967) 30.
[12] G.L. Reynolds, B. Burton, J. Nucl. Mater. 88 (1979) 22.